THE APPLICATION OF MULTIWAVELET FILTER BANKS TO IMAGE PROCESSING*

V. Strela[†,‡], P. N. Heller[‡], G. Strang[†], P. Topiwala[§], C. Heil[¶]

Abstract

Multiwavelets are a new addition to the body of wavelet theory. Realizable as matrix-valued filter banks leading to wavelet bases, multiwavelets offer simultaneous orthogonality, symmetry, and short support, which is not possible with scalar 2-channel wavelet systems. After reviewing this recently developed theory, we examine the use of multiwavelets in a filter bank setting for discrete-time signal and image processing. Multiwavelets differ from scalar wavelet systems in requiring two or more input streams to the multiwavelet filter bank. We describe two methods (repeated row and approximation/deapproximation) for obtaining such a vector input stream from a one-dimensional signal. Algorithms for symmetric extension of signals at boundaries are then developed, and naturally integrated with approximation-based preprocessing. We describe an additional algorithm for multiwavelet processing of two-dimensional signals, two rows at a time, and develop a new family of multiwavelets (the constrained pairs) that is well-suited to this approach. This suite of novel techniques is then applied to two basic signal processing problems, denoising via wavelet-shrinkage, and data compression. After developing the approach via model problems in one dimension, we applied multiwavelet processing to images, frequently obtaining performance superior to the comparable scalar wavelet transform.

EDICS category: IP 1.6

submitted to *IEEE Trans. on Image Processing*

Contact address:
Peter Niels Heller
Aware, Inc.
40 Middlesex Turnpike
Bedford, MA 01730-1432
Phone: (617) 276-4000
FAX: (617) 276-4001
email: heller@aware.com

*Work at Aware, Inc. was supported in part by the Advanced Research Projects Agency of the Department of Defense and monitored by the Air Force Office of Scientific Research under contract no. F49620-92-C-0054. Portions of this work were performed at the MITRE Corporation with the support of the MITRE Sponsored Research Project.

[†]Dartmouth College, Hanover, NH 03755

[‡]Aware Inc., Bedford, MA 01730

[§]Sanders, Inc., Nashua, NH 03061

[¶]Georgia Institute of Technology, Atlanta, GA 30332

1 Introduction

Wavelets are a useful tool for signal processing applications such as image compression and denoising. Until recently, only *scalar* wavelets were known: wavelets generated by *one* scaling function. But one can imagine a situation when there is *more than one* scaling function [16]. This leads to the notion of *multiwavelets*, which have several advantages in comparison to scalar wavelets [36]. Such features as short support, orthogonality, symmetry, and vanishing moments are known to be important in signal processing. A scalar wavelet *cannot* possess all these properties at the same time [35]. On the other hand, a multiwavelet system *can* simultaneously provide perfect reconstruction while preserving length (orthogonality), good performance at the boundaries (via linear-phase symmetry), and a high order of approximation (vanishing moments). Thus multiwavelets offer the possibility of superior performance for image processing applications, compared with scalar wavelets.

We describe here novel techniques for multirate signal processing implementations of multiwavelets, and present experimental results for the application of multiwavelets to signal denoising and image compression. The paper is organized as follows. Section 2 reviews the definition and construction of continuous-time multiwavelet systems, and Section 3 describes the connection between multiwavelets and matrix-valued multirate filterbanks. In Section 4 we develop several techniques for applying multiwavelet filter banks to one-dimensional signals, including approximation-based preprocessing and symmetric extension for finite-length signals. Two-dimensional signal processing offers a new set of problems and possibilities for the use of multiwavelets; we discuss several methods for the two-dimensional setting in Section 5, including a new family of multiwavelets, the constrained pairs. Finally, in Section 6 we describe the results of our application of multiwavelets to signal denoising and data compression.

2 Multiwavelets — several wavelets with several scaling functions

As in the scalar wavelet case, the theory of multiwavelets is based on the idea of multiresolution analysis (MRA). The difference is that multiwavelets have several scaling functions. The standard multiresolution has one scaling function $\phi(t)$:

- The translates $\phi(t-k)$ are linearly independent and produce a basis of the subspace V_0;
- The dilates $\phi(2^j t - k)$ generate subspaces V_j, $j \in \mathbf{Z}$, such that

$$\cdots \subset V_{-1} \subset V_0 \subset V_1 \subset \cdots \subset V_j \subset \cdots$$

$$\overline{\bigcup_{j=-\infty}^{\infty} V_j} = L^2(\mathbf{R}), \qquad \bigcap_{j=-\infty}^{\infty} V_j = \{0\}\,.$$

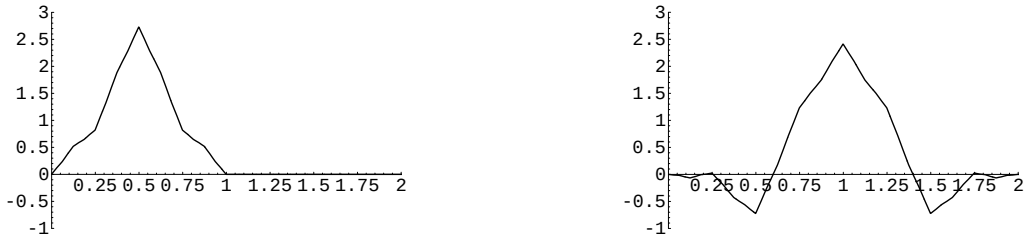

Figure 1: Geronimo–Hardin–Massopust pair of scaling functions.

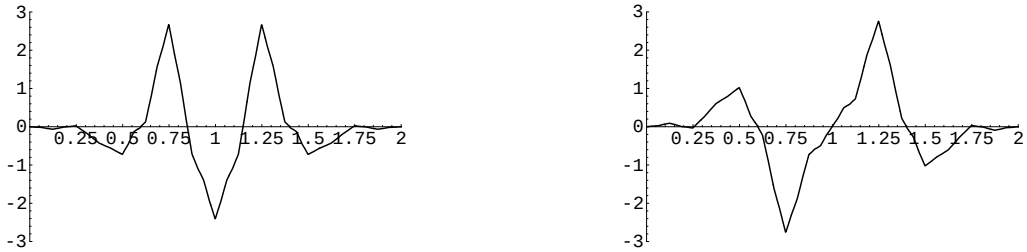

Figure 2: Geronimo–Hardin–Massopust multiwavelets.

- There is one wavelet $w(t)$. Its translates $w(t-k)$ produce a basis of the "detail" subspace W_0 to give V_1:

$$V_1 = V_0 \oplus W_0.$$

For multiwavelets, the notion of MRA is the same except that now a basis for V_0 is generated by translates of N scaling functions $\phi_1(t-k)$, $\phi_2(t-k)$, $\ldots$, $\phi_N(t-k)$. The vector $\Phi(t) = [\phi_1(t), \ldots, \phi_N(t)]^T$, will satisfy a *matrix* dilation equation (analogous to the scalar case)

$$\Phi(t) = \sum_k C[k]\Phi(2t-k). \tag{1}$$

The coefficients $C[k]$ are N by N matrices instead of scalars.

Associated with these scaling functions are N wavelets $w_1(t), \ldots, w_N(t)$, satisfying the *matrix* wavelet equation

$$W(t) = \sum_k D[k]\Phi(2t-k). \tag{2}$$

Again, $W(t) = [w_1(t), \ldots, w_N(t)]^T$ is a vector and the $D[k]$ are N by N matrices.

As in the scalar case, one can find the conditions of orthogonality and approximation for multiwavelets [36, 37, 20, 29]; this is discussed below.

A very important multiwavelet system was constructed by J. Geronimo, D. Hardin, and P. Massopust [16] (see [1] for another early multiwavelet construction). Their system contains the two scaling functions

$\phi_1(t), \phi_2(t)$ shown in Figure 1 and the two wavelets $w_1(t), w_2(t)$ shown in Figure 2. The dilation and wavelet equations for this system have four coefficients:

$$\Phi(t) = \begin{bmatrix} \phi_1(t) \\ \phi_2(t) \end{bmatrix} = C[0]\Phi(2t) + C[1]\Phi(2t-1) + C[2]\Phi(2t-2) + C[3]\Phi(2t-3)\,,$$

$$C[0] = \begin{bmatrix} \frac{3}{5} & \frac{4\sqrt{2}}{5} \\ -\frac{1}{10\sqrt{2}} & -\frac{3}{10} \end{bmatrix}, \qquad C[1] = \begin{bmatrix} \frac{3}{5} & 0 \\ \frac{9}{10\sqrt{2}} & 1 \end{bmatrix},$$

$$C[2] = \begin{bmatrix} 0 & 0 \\ \frac{9}{10\sqrt{2}} & -\frac{3}{10} \end{bmatrix}, \qquad C[3] = \begin{bmatrix} 0 & 0 \\ -\frac{1}{10\sqrt{2}} & 0 \end{bmatrix}; \tag{3}$$

$$W(t) = \begin{bmatrix} w_1(t) \\ w_2(t) \end{bmatrix} = D[0]\Phi(2t) + D[1]\Phi(2t-1) + D[2]\Phi(2t-2) + D[3]\Phi(2t-3)\,,$$

$$D[0] = \frac{1}{10}\begin{bmatrix} -\frac{1}{\sqrt{2}} & -3 \\ 1 & 3\sqrt{2} \end{bmatrix}, \qquad D[1] = \frac{1}{10}\begin{bmatrix} \frac{9}{\sqrt{2}} & -10 \\ -9 & 0 \end{bmatrix},$$

$$D[2] = \frac{1}{10}\begin{bmatrix} \frac{9}{\sqrt{2}} & -3 \\ 9 & -3\sqrt{2} \end{bmatrix}, \qquad D[3] = \frac{1}{10}\begin{bmatrix} -\frac{1}{\sqrt{2}} & 0 \\ -1 & 0 \end{bmatrix}. \tag{4}$$

There are four remarkable properties of the Geronimo-Hardin-Massopust scaling functions:

- They each have short support (the intervals [0, 1] and [0, 2]).
- Both scaling functions are symmetric, and the wavelets form a symmetric/antisymmetric pair.
- All integer translates of the scaling functions are orthogonal.
- The system has second order of approximation (locally constant and locally linear functions are in V_0).

Let us stress that a scalar system with one scaling function cannot combine symmetry, orthogonality, and second order approximation. Moreover, a solution of a scalar dilation equation with four coefficients is supported on the interval [0, 3]!

Other useful orthogonal multiwavelet systems with second order approximation are the *symmetric pair* determined by three coefficients

$$C[0] = \begin{bmatrix} 0 & \frac{2+\sqrt{7}}{4} \\ 0 & \frac{2-\sqrt{7}}{4} \end{bmatrix}, \quad C[1] = \begin{bmatrix} \frac{3}{4} & \frac{1}{4} \\ \frac{1}{4} & \frac{3}{4} \end{bmatrix}, \quad C[2] = \begin{bmatrix} \frac{2-\sqrt{7}}{4} & 0 \\ \frac{2+\sqrt{7}}{4} & 0 \end{bmatrix}$$

and the *Chui-Lian pair* [6] determined by the coefficients

$$C[0] = \begin{bmatrix} \frac{1}{2} & -\frac{1}{2} \\ \\ \frac{\sqrt{7}}{4} & -\frac{\sqrt{7}}{4} \end{bmatrix}, \quad C[1] = \begin{bmatrix} 2 & 0 \\ \\ 0 & 1 \end{bmatrix}, \quad C[2] = \begin{bmatrix} \frac{1}{2} & \frac{1}{2} \\ \\ -\frac{\sqrt{7}}{4} & -\frac{\sqrt{7}}{4} \end{bmatrix}. \tag{5}$$

Corresponding scaling functions are shown in Figures 3 and 4. Observe that for the symmetric pair one scaling function is the reflection of the other about its center point. Moreover, the Chui-Lian symmetric/antisymmetric scaling functions are the sum and difference of the two functions from the symmetric pair. In this article we will make use of several other nonsymmetric multiwavelets with desirable properties. More on the construction of multiscaling functions and multiwavelets can be found in [1, 9, 13, 18, 22, 24, 30, 31, 38, 39, 41].

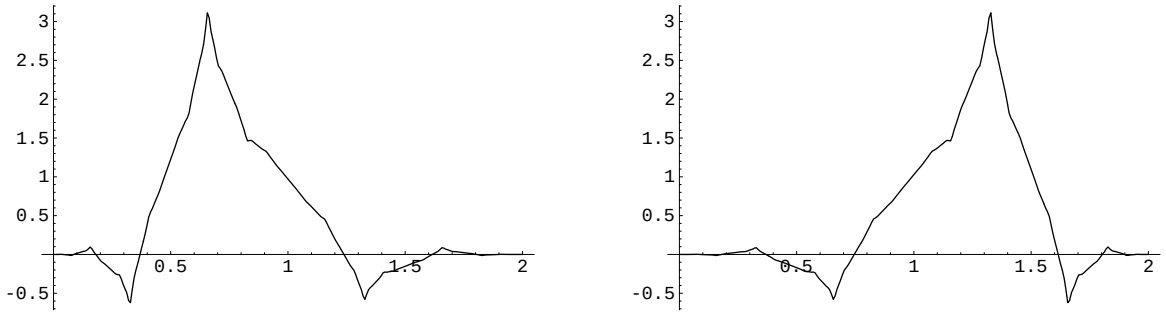

Figure 3: Symmetric pair of orthogonal scaling functions.

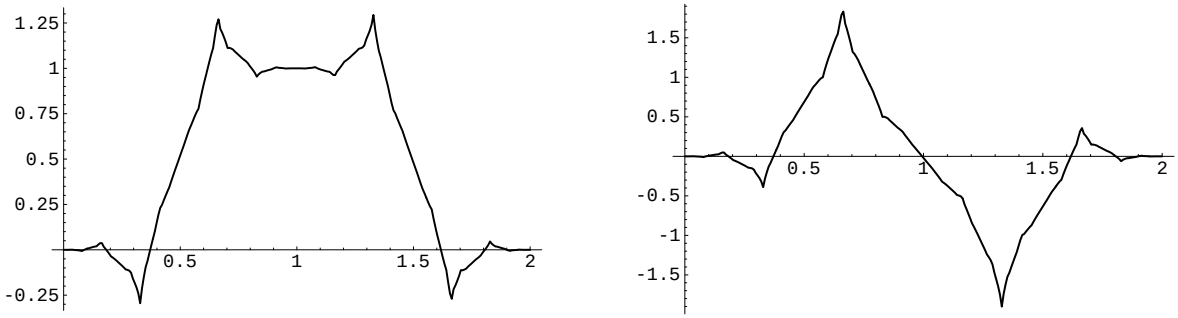

Figure 4: Chui-Lian symmetric/antisymmetric orthogonal scaling functions.

3 Multiwavelets and multirate filter banks

Corresponding to each multiwavelet system is a matrix-valued multirate filter bank [15], or multifilter. A multiwavelet filter bank [36] has "taps" that are $N \times N$ matrices (in this paper, we will be working with $N = 2$). Our principal example is the 4-coefficient symmetric multiwavelet filter bank whose lowpass filter was reported in [16]. This filter is given by the four 2×2 matrices $C[k]$ of equation (3). Unlike a scalar 2-band paraunitary filter bank, the corresponding highpass filter (specified by the four 2×2 matrices $D[k]$ of equation (4)) cannot be obtained simply as an "alternating flip" of the lowpass filter; the wavelet filters $D[k]$ must be designed [36]. The resulting 2-channel, 2×2 matrix filter bank operates on *two* input data streams, filtering them into *four* output streams, each of which is downsampled by a factor of 2. This is shown in Figure 5. Each row of the multifilter is a combination of two ordinary filters, one operating on the first data stream and the other operating on the second. For example, the first lowpass multiwavelet filter given in (3) operates as $c_{0,0}[k]$ on the first input stream and $c_{0,1}[k]$ on the second. It is a combination of the Haar filter $\{1, 1\}$ on the first stream and the unit impulse response on the second stream.

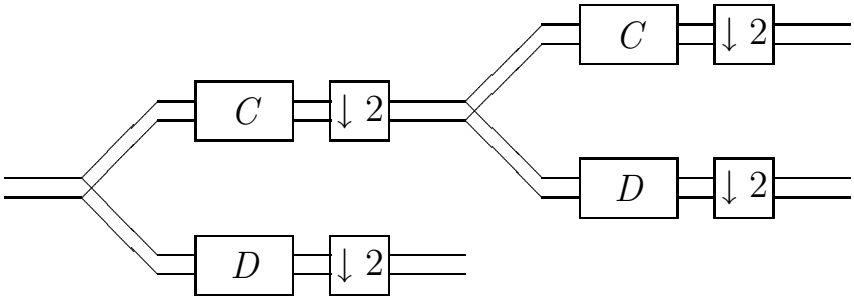

Figure 5: A multiwavelet filter bank, iterated once.

We ask that the matrix filter coefficients satisfy the orthogonality ("block-paraunitarity") condition

$$\sum_{k=0}^{N-1} C[k]\, C[k-2l]^T = 2\delta_{0,l}\, I\ . \tag{6}$$

In the time domain, filtering followed by downsampling is described by an infinite lowpass matrix with double shifts:

$$L = \begin{bmatrix} \cdots & & & & & & & \\ & C[3] & C[2] & C[1] & C[0] & 0 & 0 & \\ & 0 & 0 & C[3] & C[2] & C[1] & C[0] & \\ & & & & & & & \cdots \end{bmatrix}\ .$$

Each of the filter taps $C[k]$ is a 2×2 matrix. The eigenvalues of the matrix L are critical. The solution to the matrix dilation equation (1) is a two-element vector of scaling functions $\Phi(t) = [\phi_1(t), \phi_2(t)]^T$. The

span of integer translates of the multiwavelet scaling functions is the "lowpass" space V_0, the set of scale-limited signals [17]. Any continuous-time function $f(t)$ in V_0 can be expanded as a linear combination

$$f(t) = \sum_n v_{1,n}^{(0)}\,\phi_1(t-n) + v_{2,n}^{(0)}\,\phi_2(t-n)\,.$$

The superscript (0) denotes an expansion "at scale level 0." $f(t)$ is completely described by the sequences $\left\{v_{1,n}^{(0)}\right\}$, $\left\{v_{2,n}^{(0)}\right\}$. Given such a pair of sequences, their coarse approximation (component in V_{-1}) is computed with the lowpass part of the multiwavelet filter bank:

$$\begin{bmatrix} \vdots \\ \begin{bmatrix} v_{1,n}^{(-1)} \\ v_{2,n}^{(-1)} \end{bmatrix} \\ \begin{bmatrix} v_{1,n+1}^{(-1)} \\ v_{2,n+1}^{(-1)} \end{bmatrix} \\ \vdots \end{bmatrix} = L \begin{bmatrix} \vdots \\ \begin{bmatrix} v_{1,n}^{(0)} \\ v_{2,n}^{(0)} \end{bmatrix} \\ \begin{bmatrix} v_{1,n+1}^{(0)} \\ v_{2,n+1}^{(0)} \end{bmatrix} \\ \vdots \end{bmatrix}.$$

Because the multifilter $C[k]$ is FIR, each apparently infinite sum in the matrix multiplication is actually finite and well-defined. Analogously, the details $w_{1,n}^{(-1)}$, $w_{2,n}^{(-1)}$ in W_{-1} are computed with the highpass part $D[k]$. Thus the multiwavelet filter bank plays the same mediating role in multiresolution analysis that a scalar filter bank plays for scalar wavelet systems. If the matrix L has eigenvalues $1, \frac{1}{2}, \ldots, \frac{1}{2^{p-1}}$ and the corresponding eigenvectors have a special form, then polynomials of degree less than p belong to the space V_0 [20, 29]. This holds for the Geronimo-Hardin-Massopust multiwavelet filter with $p = 2$; linear functions can be exactly represented as linear combinations of integer translates of the scaling functions ϕ_1 and ϕ_2.

4 One-dimensional signal processing with multiwavelet filter banks

The lowpass filter C and highpass filter D consist of coefficients corresponding to the dilation equation (1) and wavelet equation (2). But in the multiwavelet setting these coefficients are n by n matrices, and during the convolution step they must multiply vectors (instead of scalars). This means that multifilter banks *need n input rows*. We will consider several ways to produce those rows. In this section the signals are one-dimensional; in the next section we consider two-dimensional signal processing.

4.1 Oversampled scheme

The most obvious way to get two input rows from a given signal is to repeat the signal. Two identical rows go into the multifilter bank. This procedure, which we call "repeated row," is shown in Figure 6. It

introduces oversampling of the data by a factor of two. Oversampled representations have proven useful in feature extraction; however, they require more calculation than critically-sampled representations. Furthermore, in data compression applications, one is seeking to remove redundancy, not increase it. In the case of one-dimensional signals the "repeated row" scheme is convenient to implement, and our experiments on denoising of one-dimensional signals were encouraging (see Section 6.1). In two dimensions the oversampling factor increases to four, limiting the usefulness of this scheme to applications such as denoising which do not require critically-sampled or near-critically-sampled representation of the data.

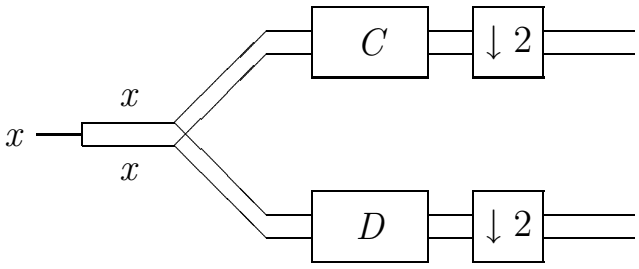

Figure 6: Multiwavelet filter bank with "repeated row" inputs.

4.2 A critically-sampled scheme: approximation-based preprocessing

A different way to get input rows for the multiwavelet filter bank is to *preprocess* the given scalar signal $f[n]$. For data compression, where one is trying to find compact transform representations for a dataset, it is imperative to find critically sampled multiwavelet transform schemes. We describe a preprocessing algorithm based on the approximation properties of the continuous-time multiwavelets which yields a critically sampled signal representation. We develop this scheme (suggested to us by J. Geronimo) in the context of Geronimo-Hardin-Massopust multiwavelets; however, it works equally well for the Chui-Lian multiwavelets with minor modifications.

Let the continuous-time function $f(t)$ belong to the scale-limited subspace V_0 generated by translates of the GHM scaling functions. This means that $f(t)$ is a linear combination of translates of those functions:

$$f(t) = \sum_n v_{1,n}^{(0)}\, \phi_1(t-n) + v_{2,n}^{(0)}\, \phi_2(t-n)\,. \tag{7}$$

Suppose that the input sequence $f[n]$ contains samples of $f(t)$ at half integers:

$$f[2n] = f(n), \qquad f[2n+1] = f(n+1/2).$$

$\phi_1(t)$ vanishes at all integer points. $\phi_2(t)$ is nonzero only at the integer 1. Sampling the relation (7) at

integers and half integers gives

$$\begin{aligned} f[2n] &= \phi_2(1)\, v^{(0)}_{2,n-1}\,, \\ f[2n+1] &= \phi_2(3/2)\, v^{(0)}_{2,n-1} + \phi_1(1/2)\, v^{(0)}_{1,n} + \phi_2(1/2)\, v^{(0)}_{2,n}. \end{aligned} \tag{8}$$

The coefficients $v^{(0)}_{1,n},\ v^{(0)}_{2,n}$ can be easily found from (8):

$$\begin{aligned} v^{(0)}_{1,n} &= \tfrac{\phi_2(1)\, f[2n+1] - \phi_2(1/2)\, f[2n+2] - \phi_2(3/2)\, f[2n]}{\phi_2(1)\, \phi_1(1/2)}\,, \\ v^{(0)}_{2,n} &= \tfrac{f[2n+2]}{\phi_2(1)}. \end{aligned}$$

Taking into account the symmetry of $\phi_2(t)$, we finally get

$$\begin{aligned} v^{(0)}_{1,n} &= \tfrac{\phi_2(1)\, f[2n+1] - \phi_2(1/2)\, (f[2n+2] + f[2n])}{\phi_2(1)\, \phi_1(1/2)}\,, \\ v^{(0)}_{2,n} &= \tfrac{f[2n+2]}{\phi_2(1)}\ . \end{aligned} \tag{9}$$

The relations (9) give a natural way to get two input rows $v^{(0)}_{1,n}$, $v^{(0)}_{2,n}$ starting from a given signal $f[n]$. To synthesize the signal on output we invert (9) and recover (8). This sequence of operations is depicted in Figure 7.

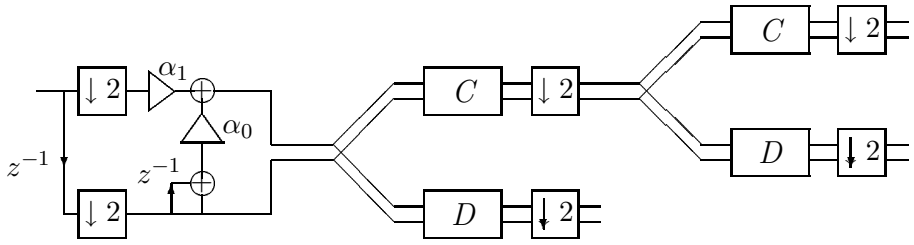

Figure 7: Approximation-based preprocessing and two steps of filtering for one-dimensional signals.

In the case of Chui-Lian multiwavelets, the only difference from the above approach is that $\phi_1(1) = 1$ and $\phi_2(1) = 0$, so that we use the samples of f at the integers to determine the coefficients $v^{(0)}_{1,n}$ and then find the $v^{(0)}_{2,n}$ from the samples of f at the half-integers.

Given any $f(t) \in V_0$, the preprocessing step (9) followed by filtering will produce nontrivial output in the lowpass branch only. It yields zero output in the highpass subband. For example, $f(t) \equiv 1$ (locally in V_0) gives $v^{(0)}_{1,n} = 1$ and $v^{(0)}_{2,n} = \sqrt{2}$, which is the eigenvector of the matrix L^T with eigenvalue 1.

This preprocessing algorithm also maintains a critically sampled representation: if the data enters at rate R, preprocessing yields two streams at rate $R/2$ for input to the multifilter, which produces four output streams, each at a rate $R/4$.

Another advantage of this approximation-based preprocessing method is that it fits naturally with symmetric extension for multiwavelets (discussed below in Subsection 4.3). In other words, if we symmetrically extend a finite length signal $f[n]$ at its boundaries and implement the approximation formulas (9), then the two rows $v^{(0)}_{1,n}, v^{(0)}_{2,n}$ from the preprocessor will have the appropriate symmetry.

One also can develop a general approximation-type preprocessing based on the following idea. Suppose again that our given signal f lies in V_0. This implies that

$$f(t) = \sum_{n,k} v_{k,n}^{(0)} \, \phi_k(t - n). \tag{10}$$

The goal of preprocessing is to find the coefficients $v_{k,n}^{(0)}$ from the signal samples.

Assume that a multiwavelet system has N scaling functions, all supported on $[0, 1]$. Now restrict equation (10) to this interval:

$$f(t) = \sum_{k} v_{k,0}^{(0)} \, \phi_k(t) \; , \qquad 0 \le t \le 1. \tag{11}$$

Suppose that samples $f[0], \ldots, f[N-1]$ are the values of the function $f(t)$ at the points

$$t \, = \, \frac{1}{2N}, \, \frac{3}{2N}, \, \ldots, \, \frac{2N-1}{2N} \, .$$

The representation (11) gives a linear system for the coefficients $v_{0,0}^{(0)}, \ldots, v_{N-1,0}^{(0)}$. The following N samples $f[N], \ldots, f[2N-1]$ give the values of $v_{0,1}^{(0)}, \ldots, v_{N-1,1}^{(0)}$. Repeating this procedure we find all the $v_{k,n}^{(0)}$. If some of the scaling functions have support longer than $[0, 1]$, we will need several initial (boundary) values of $v_{k,-1}^{(0)}, v_{k,-2}^{(0)}, \ldots$. In the case of finite length signals, these numbers can be obtained from the conditions of periodization or symmetric extension (Section 4.3). Other multiwavelet preprocessing techniques are discussed in [7, 19, 27, 41, 43, 44, 45, 46].

4.3 Symmetric extension of finite-length signals

In practice all signals have finite length, so we must devise techniques for filtering such signals at their boundaries. There are two common methods for filtering at the boundary that preserve critical sampling. The first is circular periodization (periodic wrap) of the data. This method introduces discontinuities at the boundaries; however, it can be used with almost any filter bank. The second approach is symmetric extension of the data. Symmetric extension preserves signal continuity, but can be implemented only with linear-phase (symmetric and/or antisymmetric) filter banks [34, 3, 23, 4]. We now develop symmetric extension for linear-phase multiwavelet filters, such as the Geronimo-Hardin-Massopust and Chui-Lian multifilters. This proves useful for image compression applications (Section 6).

Recall the basic problem: given an input signal $f[n]$ with N samples and a linear-phase (symmetric or antisymmetric) filter, how can we symmetrically extend f before filtering and downsampling in a way that preserves the critically sampled nature of the system? The possibilities for such an extension have been enumerated in [4]. Depending on the parity of the input signal (even- or odd-length) and the parity and symmetry of the filter, there is a specific non-expansive symmetric extension of both the input signal and the subband outputs. For example, an even-length input signal passed through an even-length

symmetric lowpass filter should be extended by repeating the first and last samples, i.e., a half-sample symmetric signal is matched to a half-sample-symmetric filter. Similarly, when the lowpass filter is of odd length (whole-sample-symmetry), the input signal should be extended without repeating the first or last samples.

Each row of the GHM multifilter (equations (3) and (4)) is a linear combination of two filters, one for each input stream. One filter (applied to the first stream) is of even length; the second is of odd length. Thus we should extend the first stream using half-sample-symmetry (repeating the first and last samples) and extend the second stream using whole-sample-symmetry (*not* repeating samples). Then, when synthesizing the input signal from the subband outputs, we must symmetrize the subband data differently depending on whether it is going into an even- or odd-length filter.

In particular suppose we are given two input rows (one of even length, the other of odd length):

$$\begin{matrix} v_{1,0}^{(0)} & v_{1,1}^{(0)} & v_{1,2}^{(0)} & \dots & v_{1,N-1}^{(0)} & \\ v_{2,0}^{(0)} & v_{2,1}^{(0)} & v_{2,2}^{(0)} & \dots & v_{2,N-1}^{(0)} & v_{2,N}^{(0)} \end{matrix} .$$

If they are symmetrically extended as

$$\begin{matrix} \dots & v_{1,1}^{(0)} & v_{1,0}^{(0)} & v_{1,0}^{(0)} & v_{1,1}^{(0)} & \dots \\ \dots & v_{2,1}^{(0)} & v_{2,0}^{(0)} & v_{2,1}^{(0)} & v_{2,2}^{(0)} & \dots \end{matrix} \tag{12}$$

at the start and

$$\begin{matrix} \dots & v_{1,N-2}^{(0)} & v_{1,N-1}^{(0)} & v_{1,N-1}^{(0)} & \dots \\ \dots & v_{2,N-1}^{(0)} & v_{2,N}^{(0)} & v_{2,N-1}^{(0)} & \dots \end{matrix} \tag{13}$$

at the end to give two symmetric rows, then after one step of the cascade algorithm we have the four symmetric subband outputs:

$$\begin{matrix} \dots & v_{1,1}^{(-1)} & v_{1,0}^{(-1)} & v_{1,0}^{(-1)} & \dots & v_{1,\frac{N}{2}-2}^{(-1)} & v_{1,\frac{N}{2}-1}^{(-1)} & v_{1,\frac{N}{2}-1}^{(-1)} & \dots \\ \dots & v_{2,1}^{(-1)} & v_{2,0}^{(-1)} & v_{2,1}^{(-1)} & \dots & v_{2,\frac{N}{2}-1}^{(-1)} & v_{2,\frac{N}{2}}^{(-1)} & v_{2,\frac{N}{2}-1}^{(-1)} & \dots \\ \dots & w_{1,1}^{(-1)} & w_{1,0}^{(-1)} & w_{1,1}^{(-1)} & \dots & w_{1,\frac{N}{2}-1}^{(-1)} & w_{1,\frac{N}{2}}^{(-1)} & w_{1,\frac{N}{2}-1}^{(-1)} & \dots \\ \dots & -w_{2,1}^{(-1)} & 0 & w_{2,1}^{(-1)} & \dots & w_{2,\frac{N}{2}-1}^{(-1)} & 0 & -w_{2,\frac{N}{2}-1}^{(-1)} & \dots \end{matrix}$$

The application of the (linear-phase) multiwavelet synthesis filters now yields the symmetric extension of the original signal.

Multiwavelet symmetric extension can be done not only for linear-phase filters. For example, the symmetric pair of scaling functions shown in Figure 3 admits the following extension of input data rows

$v_{1,k}^{(0)}$ and $v_{2,k}^{(0)}$:

$$\begin{array}{cccccccccccc} \cdots & v_{2,1}^{(0)} & v_{2,0}^{(0)} & a & v_{1,0}^{(0)} & v_{1,0}^{(0)} & v_{1,1}^{(0)} & \cdots & v_{1,N-1}^{(0)} & a & v_{2,N-1}^{(0)} & \cdots \\ \cdots & v_{1,1}^{(0)} & v_{1,0}^{(0)} & a & v_{2,0}^{(0)} & v_{2,1}^{(0)} & v_{2,2}^{(0)} & \cdots & v_{2,N-1}^{(0)} & a & v_{1,N-1}^{(0)} & \cdots \end{array} .$$

The placeholder a is an arbitrary real number. After filtering and downsampling of this extended data, the output rows will have the same symmetry. In this way we obtain a non-expansive transform of finite-length input data which behaves well at the boundaries under lossy quantization.

4.4 Computational complexity

We briefly compare the computational demands of multiwavelet and scalar wavelet filtering. One level of the cascade algorithm with the GHM multifilter does require slightly more floating point operations than the D_4 scalar wavelet. General convolution with four 2 by 2 matrix coefficients requires 16 multiplications and 14 additions to yield two outputs. However, in the case of the GHM multifilter, the presence of many zero coefficients and the linear-phase symmetry may be exploited to reduce the computation to 8 multiplies and 8 additions for the lowpass filter and 9 multiplications, 11 additions, and 2 sign-flips for the highpass filter, requiring a total of 17 multiplications, 19 additions, and 2 sign-flips (38 FLOPS total) for four output values. This amounts to 4.25 multiplications and 9.5 FLOPS per output, compared with 4 multiplications and 7 FLOPS per output for the D_4 scalar wavelet filter and 2.5 multiplications and 5.5 FLOPS for the (3,5)-tap linear-phase scalar wavelet of LeGall and Tabatabai. These complexity figures do not take into account the approximation/deapproximation processing, if any.

5 Two-dimensional signal processing with multiwavelet filter banks

Multiwavelet filtering of images needs two-dimensional algorithms. One class of such algorithms is derived simply by taking tensor products of the one-dimensional methods described in the previous section. Another class of algorithms stems from using the matrix filters of the multiwavelet system for fundamentally two-dimensional processing. We discuss each of these alternatives now.

5.1 Separable schemes based on one-dimensional methods

Section 4 described two different ways to decompose a one-dimensional signal using multiwavelets. Each of these can be turned into a two-dimensional algorithm by taking a tensor product, i.e., by performing the 1D algorithm in each dimension separately.

Suppose our 2D data is represented as an N by N matrix I_0. The first step is to preprocess all the rows and store the result as a square array I_1 such that the first half of each row contains coefficients corresponding to the first scaling function and the second half contains coefficients corresponding to the

second scaling function. The next operation is preprocessing of the columns of the array I_1 to produce an output matrix I_2, such that the first half of each column of I_2 contains coefficients corresponding to the first scaling function and the second half of each column corresponds to the second scaling function. Then the multiwavelet cascade starts – it consists of iterative low and high-pass filtering of the scaling coefficients in horizontal and vertical directions. The result after one cascade step can be realized as the following matrix:

$$\begin{array}{cccc} L_1L_1 & L_2L_1 & H_1L_1 & H_2L_1 \\ L_1L_2 & L_2L_2 & H_1L_2 & H_2L_2 \end{array}$$

$$\begin{array}{cccc} L_1H_1 & L_2H_1 & H_1H_1 & H_2H_1 \\ L_1H_2 & L_2H_2 & H_1H_2 & H_2H_2 \end{array}$$

Here a typical block H_2L_1 contains low-pass coefficients corresponding to the first scaling function in the horizontal direction and high-pass coefficients corresponding to the second wavelet in the vertical direction. The next step of the cascade will decompose the "low-low-pass" submatrix $\begin{array}{cc} L_1L_1 & L_2L \\ L_1L_2 & L_2L_2 \end{array}$ in a similar manner.

As noted before, the separable product of one-dimensional "repeated row" algorithms leads to a 4:1 data expansion, restricting the utility of this approach to applications such as denoising by thresholding, for which critical sampling is irrelevant. The separable product of the approximation-based preprocessing methods described in Section 4.2 yields a critically sampled representation, potentially useful for both denoising and data compression.

5.2 Constrained multiwavelets

A different approach to two-dimensional multiwavelet filtering is to make use of the two-dimensionality of the matrix filter coefficients. When processing an image with a scalar filterbank one usually uses as input the rows and columns of the image. For a multiwavelet system we need n input signals. Where can we get them? The first solution which comes to mind is very simple: just use n adjacent rows as the input. For the 2×2 multiwavelets used here, this would mean taking two rows of the image at a time, and applying the matrix filter coefficients to the sequence of 2-element vectors in the input stream.

However, a naive implementation of this approach does not lead to good results (see Table 4 in Section 6.4). This is due to the intricacies of multiwavelet approximation. Approximation of degree p is important for image compression because locally polynomial data can be captured in a few lowpass coefficients. A wavelet system (scalar or multiwavelet) satisfies approximation of degree p (or accuracy p) if polynomials of degree less than p belong to the scale-limited space V_0. Image data is often locally well-approximated by constant, linear, and quadratic functions; thus, such local approximations remain in the lowpass space V_0 after filtering and downsampling. This is one reason why simply retaining the

lowpass coefficients of a wavelet decomposition with accuracy p (p vanishing moments) produces good results while compressing the image representation into very few coefficients [47].

When applying multiwavelets to two-dimensional (image) processing, we use this notion of local approximation as a motivation — we wish to capture locally constant and linear features in the lowpass coefficients. Suppose we have a multiwavelet system generated by two scaling functions $\phi_1(t), \phi_2(t)$ with accuracy $p \geq 1$ (this would mean at least one vanishing wavelet moment in the scalar case). Then constant functions $f(t) \equiv c$ locally belong to the scale-limited space V_0. It has been shown [20] that the repeated constant 1 is an eigenvalue of the filtering and downsampling operator L, and there exists a left eigenvector

$$[\mathbf{u}_n] = \left[\ \ldots u_{1,n} \, , \ u_{2,n} \, , \ u_{1,n+1} \, , \ u_{2,n+1} \, , \ \ldots \ \right]$$

with

$$[\mathbf{u}_n] \, L = [\mathbf{u}_n] \ .$$

In fact, $u_{1,n} = u_{1,0}$ and $u_{2,n} = u_{2,0}$, so that

$$\left[\ \ldots u_{1,n} \, , \ u_{2,n} \, , \ u_{1,n+1} \, , \ u_{2,n+1} \, , \ \ldots \ \right] = \left[\ \ldots u_{1,0} \, , \ u_{2,0} \, , \ u_{1,0} \, , \ u_{2,0} \, , \ \ldots \ \right] \ .$$

In the continuous-time subspace V_0 this eigenvector leads to the constant function:

$$f(t) = c = c \sum_n \left(u_{1,n} \phi_1(t-n) + u_{2,n} \phi_2(t-n) \right) \ .$$

Assuming for the moment that our image is locally constant, we input two equal, constant rows of the image (two-dimensional signal) into the multiwavelet filter bank. The output will be zero in the highpass and a constant vector

$$\begin{bmatrix} c_1 \\ c_2 \end{bmatrix}$$

in the lowpass. If the eigenvector $[\mathbf{u}_n]$ of L satisfies $u_{1,0} = u_{2,0}$, then we will get $c_1 = c_2$ and the constant input yields a constant lowpass output. However, there is no guarantee of this happy state; for example, in the case of the Geronimo-Hardin-Massopust multiwavelet (3),

$$\begin{bmatrix} u_{1,0} & u_{2,0} \end{bmatrix} \ \propto \ \begin{bmatrix} 1 & \sqrt{2} \end{bmatrix}$$

and therefore $c_1 \neq c_2$. Thus the lowpass responses of an arbitrary multifilter to a constant input are *different* constants. Quantization of these lowpass multifilter outputs (for lossy compression) will then introduce a rippled texture in the lowpass part of the image, creating unacceptable artifacts. This is borne out by experiments using the GHM multifilter (Section 6.4 below).

Similar arguments hold for linear approximation [20]: a multiwavelet system has linear approximation (accuracy of order $p = 2$) if and only if there are two left eigenvectors. The first is

$$[\mathbf{u}_n] = \left[\ \ldots \, u_{1,0} \, , \ u_{2,0} \, , \ u_{1,0} \, , \ u_{2,0} \, , \ \ldots \ \right]$$

satisfying

$$[\mathbf{u}_n]\, L = [\mathbf{u}_n] \ .$$

as before. The second eigenvector is

$$[\mathbf{v}_n] = \left[\ \ldots \, v_{1,n} \, , \ v_{2,n} \, , \ v_{1,n+1} \, , \ v_{2,n+1} \, , \ \ldots \ \right]$$

also satisfying

$$[\mathbf{v}_n]\, L = [\mathbf{v}_n] \ .$$

For linear approximation we must have

$$v_{1,n} = y_{1,0} - n u_{1,0}$$

and

$$v_{2,n} = y_{2,0} - n u_{2,0}$$

for some constants $y_{1,0}$ and $y_{2,0}$, so that

$$[\mathbf{v}_n] = \left[\ \ldots \, y_{1,0} - n u_{1,0} \, , \ y_{2,0} - n u_{2,0} \, , \ y_{1,0} - (n+1) u_{1,0} \, , \ y_{2,0} - (n+1) u_{2,0} \, , \ \ldots \ \right] \ .$$

This second eigenvector leads to linear approximation; indeed,

$$g(t) = t = \sum_n v_{1,n} \phi_1(t-n) + v_{2,n} \phi_2(t-n) \ .$$

Again, there is no reason to expect that $y_{1,0} = y_{2,0}$, and so if we input two equal linear rows into the multifilter, they will most likely emerge as two *different* linear rows. Thus the locally linear nature of many images will become distorted under such a multiwavelet transform, and this distortion will lead to unacceptable artifacts under quantization.

One way to avoid this phenomenon is to construct a multiwavelet system in which the eigenvectors have pairwise equal components

$$[\mathbf{u}_n] \ = \ \left[\ \ldots \, u_{1,0} \, , \ u_{1,0} \, , \ u_{1,0} \, , \ \ldots \ \right] \tag{14}$$

$$[\mathbf{v}_n] \ = \ \left[\ \ldots \, y_{1,0} - n u_{1,0} \, , \ y_{1,0} - n u_{1,0} \, , \ y_{1,0} - (n+1) u_{1,0} \, , \ y_{1,0} - (n+1) u_{1,0} \, , \ \ldots \ \right] \ , \tag{15}$$

which produce two equal linear outputs as the response to two equal linear inputs. Such multiwavelets can be constructed, but as we will see, the restrictions (14) and (15) imply some constraints on the properties of the multiscaling functions.

Consider a multiwavelet system with two scaling functions satisfying a matrix dilation equation with four coefficients

$$\Phi(t) \ = \ \begin{bmatrix} \phi_1(t) \\ \phi_2(t) \end{bmatrix} \tag{16}$$

$$= \ C[0]\Phi(2t) + C[1]\Phi(2t-1) + C[2]\Phi(2t-2) + C[3]\Phi(2t-3) \ .$$

It is proven in [20] that the vectors $u = [u_{1,0} \quad u_{2,0}]$, $y = [y_{1,0} \quad y_{2,0}]$ must satisfy the following system of equations:

$$\begin{aligned} & u\,(C[0] + C[2]) = u \\ & u\,(C[1] + C[3]) = u \\ & yC[1] + (u+y)C[3] = \tfrac{1}{2}y \\ & yC[0] + (u+y)C[2] = \tfrac{1}{2}(u+y)\ . \end{aligned} \tag{17}$$

We want

$$u_{1,0} = u_{2,0} = u_0\,, \tag{18}$$

and

$$y_{1,0} = y_{2,0} = y_0\,, \tag{19}$$

i.e., $y = (y_0/u_0)\,u$. From the dilation equation (16) and the approximation constraints (17), it follows that u is a mutual eigenvector of all four matrices $C[k]$:

$$u\,C[k] = c'_k u,\ k = 0,\,1,\,2,\,3\,. \tag{20}$$

Consider now a scalar function $\phi(t)$

$$\phi(t) = \frac{1}{u_0} u\,\Phi(t) = \phi_1(t) + \phi_2(t).$$

According to (16) and (20), $\phi(t)$ satisfies the scalar dilation equation

$$\phi(t) = c'_0\phi(2t) + c'_1\phi(2t-1) + c'_2\phi(2t-2) + c'_3\phi(2t-3).$$

The only solution to this equation with orthogonal translates and second order of approximation is Daubechies' D_4 scaling function [10]. Thus any orthogonal pair $\{\phi_1\,,\ \phi_2\}$ which has second order of approximation, satisfies the dilation equation (16), and the eigenvector constraints (18) — (19) must sum to D_4:

$$\phi_1(t) + \phi_2(t) = D_4(t).$$

We call such pairs "constrained" multiscaling functions. There are infinitely many constrained orthogonal solutions of (20). Plots of two of them are shown in Figures 8 and 9. The ideas similar to those underlying "constrained" multiwavelets were used in [25] in order to construct different types of "balanced" multiwavelets.

The implementation of constrained multiwavelets for the two-dimensional wavelet transform is straightforward. In each step of Mallat's algorithm [26], one first processes pairs of rows and then pairs of columns. Because locally constant and linear data are passed through to the lowpass ouputs of a constrained multifilter, the performance of these constrained multiwavelets in image compression is much better than that of the "non-constrained" GHM pair, when applied by using two adjacent rows as the input. This is confirmed by the experiments reported in the next section, as shown in Tables 4 and 5.

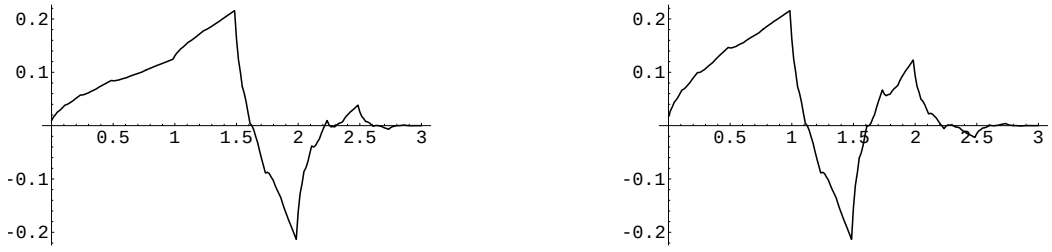

Figure 8: Constrained Pair 1.

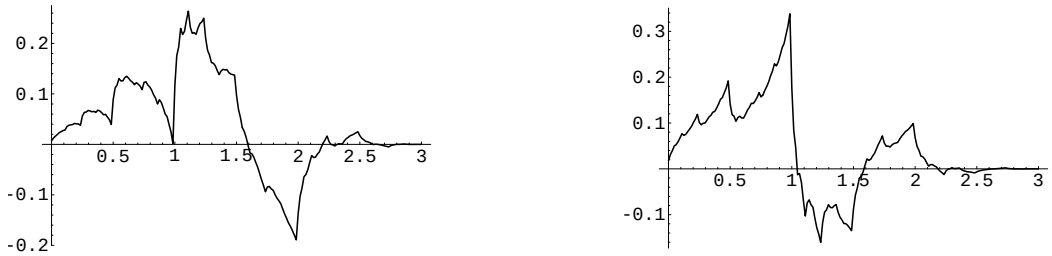

Figure 9: Constrained Pair 2.

6 Signal processing applications of multiwavelets

In this section we are going to compare the numerical performance of GHM and constrained multiwavelets with Daubechies D_4 scalar wavelets. We perform these comparisons in two standard wavelet applications: signal denoising and data compression. We first develop these applications for one-dimensional signals, then extend them to images. D_4 wavelets were chosen because they have two vanishing moments, are orthogonal and have four coefficients in the dilation equation — exactly like the GHM and constrained pairs. For the application to image coding, we also add the (3,5)-tap scalar wavelet of LeGall and Tabatabai to the mix. It has second-order approximation as well as linear-phase symmetry, at the cost of biorthogonality instead of orthogonality.

6.1 Denoising by thresholding

Suppose that a signal of interest f has been corrupted by noise, so that we observe a signal g:

$$g[n] = f[n] + \sigma z[n], \quad n = 0\,, 1, \ldots, N-1\,.$$

where $z[n]$ is unit-variance, zero-mean Gaussian white noise. What is a robust method for recovering f from the samples $g[n]$ as best as possible? Donoho and Johnstone [11, 12] have proposed a solution via wavelet shrinkage or thresholding in the wavelet domain. Wavelet shrinkage works as follows:

1. Apply J steps of the cascade algorithm to get the $N - N/2^J$ wavelet coefficients and $N/2^J$ scaling coefficients corresponding to $g[n]$.

2. Choose a threshold $t_N = \sigma\sqrt{2\log(N)}$ and apply thresholding to the wavelet coefficients (leave the scaling coefficients alone).

3. Invert the cascade algorithm to get the denoised signal $\hat{f}[n]$.

We use hard thresholding when a wavelet coefficient w_{jk} stays unchanged if $w_{jk} \geq t_N$ and is set to zero if $w_{jk} < t_N$. Donoho and Johnstone's algorithm offers the advantages of smoothness and adaptation. Wavelet shrinkage is *smooth* in the sense that the denoised estimate $\hat{f}$ has a very high probability of being as smooth as the original signal f, in a variety of smoothness spaces (Sobolev, Hölder, etc.). Wavelet shrinkage also achieves near-minimax mean-square-error among possible denoisings of f, measured over a wide range of smoothness classes. In these numerical senses, wavelet shrinkage is superior to other smoothing and denoising algorithms. Heuristically, wavelet shrinkage has the advantage of not adding "bumps" or false oscillations in the process of removing noise, because of the local and smoothness-preserving nature of the wavelet transform. Wavelet shrinkage has been successfully applied to SAR imagery as a method for clutter removal [28]. It is natural to attempt to use multiwavelets as the transform for a wavelet shrinkage approach to denoising, and compare the results with scalar wavelet shrinkage.

We implemented Donoho's wavelet shrinkage algorithm and compared the performance of the D_4 scalar wavelet transform with oversampled and critically sampled multiwavelet schemes. The length of the test signal was $N = 512$ samples. We chose $J = 4$ for the critically sampled multiwavelet method and $J = 5$ for oversampled multiwavelet method and D_4 scalar method (thus 16 scaling coefficients were left untouched). In the oversampled scheme, the first row is multiplied by $\sqrt{2}$, to better match the first eigenvector of the GHM system. The critically sampled scheme uses the formulas (9) to obtain two input rows $v_{1,n}$, $v_{2,n}$ from a single row of data. After reconstruction the two output rows $\hat{v}_{1,n}$, $\hat{v}_{2,n}$ are deapproximated using (8), to yield the output signal $\hat{f}[n]$. Boundaries are handled by symmetric data extension for the critically sampled (approximation/deapproximation) and oversampled schemes, and by circular periodization for D_4.

Results of a typical experiment are shown in Table 1 and Figure 10. In all experiments both types of GHM filter banks performed better than D_4. The "repeated row" usually gave better results than "approximation" preprocessing. This is not surprising, because "repeated row" is an oversampled data representation, and it is well known that oversampled representations are useful for feature extraction.

Detailed discussion of denoising via multiwavelet thresholding, different estimates of the threshold and more results of numerical tests can be found in [8, 40].

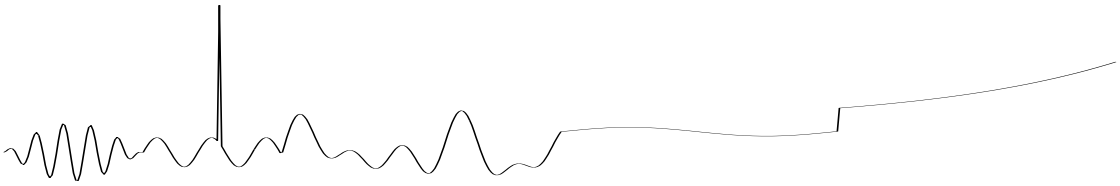

Original signal, 512 samples. Range of amplitude $[-3, 10]$

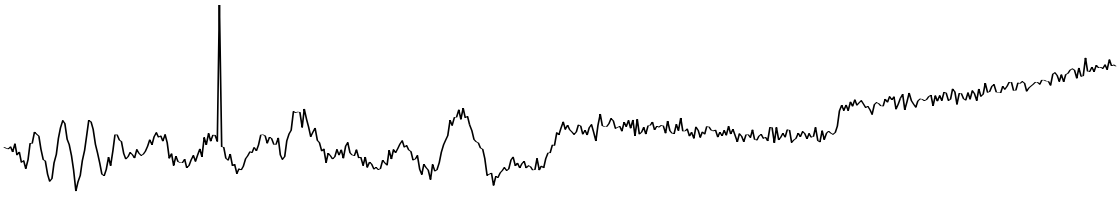

Noisy signal. Noise level $\sigma = 0.3$

Signal reconstructed using GHM with "approximation".

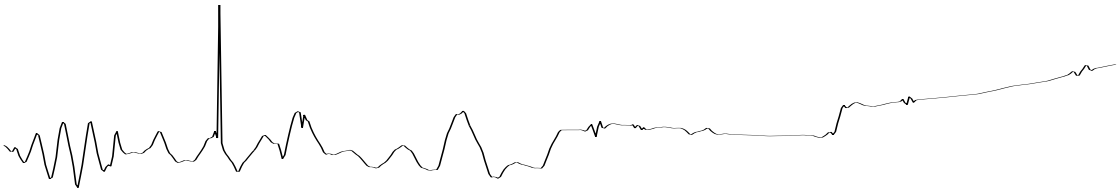

Signal reconstructed using GHM with "repeated row".

Signal reconstructed using D_4**.**

Figure 10: Denoising via wavelet-shrinkage

	Noise	GHM with approximation	GHM with repeated row	D_4
mean absolute error	0.243	0.127	0.123	0.153
root mean square error	0.300	0.196	0.177	0.227

Table 1: Denoising via wavelet soft thresholding

6.2 Thresholding for compression of one-dimensional signals

We also performed a model compression experiment, using the same one-dimensional signal as in the denoising experiments. We applied seven iterations of the cascade algorithm on this 512-point signal to get the wavelet coefficients λ_k, using the same three types of wavelet and multiwavelet filter banks. For a fair comparison, we retained the same number of the largest coefficients for each transform, then inverted the cascade algorithm to reconstruct the signal. The results are shown in Table 2 and Figure 11.

	GHM with "appr."	GHM with "rep. row"	D_4
recon with 50 largest coeffs.			
ℓ^1 error	0.1298	0.1597	0.1807
ℓ^2 (mean square) error	0.0448	0.0517	0.0815
ℓ^∞ (maximum) error	1.5709	1.0667	1.4923
recon with 75 largest coeffs.			
ℓ^1 error	0.0601	0.0650	0.0890
ℓ^2 (mean square) error	0.0091	0.0107	0.0200
ℓ^∞ (maximum) error	0.7959	0.9731	0.7301
recon with 100 largest coeffs.			
ℓ^1 error	0.0320	0.0389	0.0466
ℓ^2 (mean square) error	0.0029	0.0030	0.0049
ℓ^∞ (maximum) error	0.2821	0.2309	0.2867

Table 2: One-dimensional compression by retention of largest coefficients.

For a given number of retained coefficients, the multiwavelet transforms lead to smaller ℓ^1 (mean absolute) and ℓ^2 (root mean square) errors than the D_4 scalar wavelet transform, and comparable ℓ^∞ (maximum) errors. GHM with "approximation" is slightly superior to GHM with "repeated row". The results of this experiment led us to try using the GHM multiwavelet with "approximation" for two-dimensional image compression (with a true quantizer and coder), as discussed in Section 6.4 below.

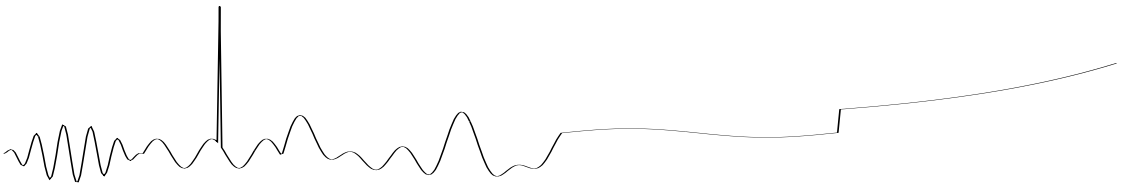

Original signal, 512 samples. Range of amplitude $[-3, 10]$

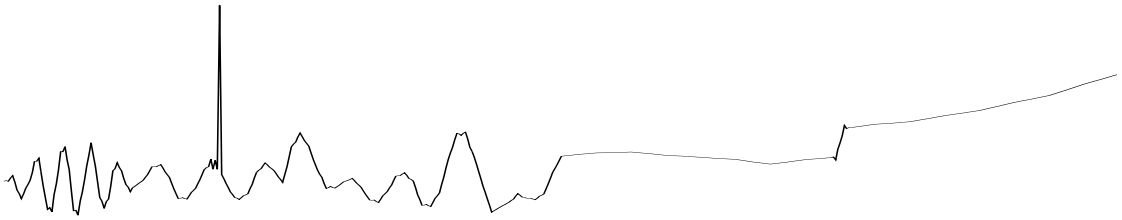

Reconstruction from 75 largest coeffs of GHM with "approximation".

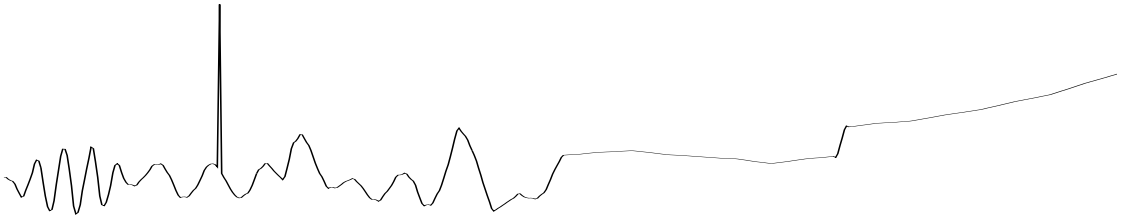

Reconstruction from 75 largest coeffs of GHM with "repeated row".

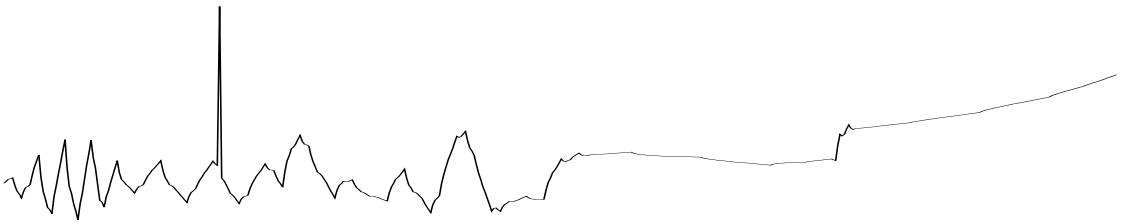

Reconstruction from 75 largest coeffs of D_4 transform.

Figure 11: One-D signal compression via retention of large coefficients.

6.3 Denoising of images

Given the success of the multiwavelets in denoising of the model one-dimensional signal, we applied multiwavelet denoising to imagery. We added white Gaussian noise with variance $\sigma = 25$ to 512 by 512 *Lena* image, and applied three wavelet transforms for denoising by wavelet shrinkage: GHM with approximation preprocessing, GHM with repeated row preprocessing, and the Daubechies 4-tap scalar wavelet. As in the 1-D case, the depth of the cascade was chosen to be $J = 4$ for GHM with approximation and $J = 5$ for GHM with repeated row and D_4. The experimental results are shown in Table 3 and in Figure 12. Multiwavelet schemes were superior to D_4 both numerically and subjectively. According to our expectations GHM with repeated row preprocessing slightly outperformed GHM with approximation-based preporcessing in terms of mean square error. Visually, multiwavelet schemes seemed to preserve the edges better (especially GHM with repeated row) and reduce the Cartesian artifacts present in the scalar wavelet shrinkage. This can be seen, for example, in the facial features (eyes, nose, lips) of the *Lena* images shown in Figure 12.

	Noise	GHM with approximation	GHM with repeated row	D_4
ℓ^1 error	19.93	7.11	7.90	8.71
ℓ^2 error	24.99	10.56	10.53	12.79

Table 3: Denoising of *Lena* image via wavelet shrinkage.

6.4 Transform-based image coding

One of the most successful applications of the wavelet transform is image compression. A transform-based coder operates by transforming the data to remove redundancy, then quantizing the transform coefficients (a lossy step), and finally entropy coding the quantizer output. Because of their energy compaction properties and correspondence with the human visual system, wavelet representations have produced superior objective and subjective results in image compression [26, 47, 2, 5]. Since a wavelet basis consists of functions with short support for high frequencies and long support for low frequencies, large smooth areas of an image may be represented with very few bits, and detail added where it is needed. Multiwavelet decompositions offer all of these traditional advantages of wavelets, as well as the combination of orthogonality, short support, and symmetry. The short support of multiwavelet filters limits ringing artifacts due to subsequent quantization. Symmetry of the filter bank not only leads to efficient boundary handling, it also preserves centers of mass, lessening the blurring of fine-scale features. Orthogonality is useful because it means that rate-distortion optimal quantization strategies may be employed in the transform domain and still lead to optimal time-domain quantization, at least when error is measured in a mean-square sense. Thus it is natural to consider the use of multiwavelets in a

Lena image with Gaussian noise MSE 24.99

GHM with approximation multiwavelet denoising, MSE 10.56

Daubechies 4 scalar wavelet denoising, MSE 12.79

GHM repeated row multiwavelet denoising, MSE 10.53

Figure 12: Multiwavelet denoising

transform-based image coder.

We employed a production image coder to compare the two-dimensional multiwavelet algorithms of Section 5 with two scalar wavelets: the Daubechies 4-tap orthogonal wavelet and the (3,5)-tap symmetric QMF of LeGall and Tabatabai. Five types of wavelet transform were used:

- (3,5)-tap scalar wavelet
- D_4 scalar wavelet
- Approximation-based preprocessing with GHM multiwavelets
- Approximation-based preprocessing with Chui-Lian multiwavelets
- Adjacent rows input with the constrained pair #1 multiwavelet
- Adjacent rows input with the constrained pair #2 multiwavelet

Each of these wavelet transforms was followed by entropy-constrained scalar quantization and entropy coding. We made the assumption that the histograms of subband (or wavelet transform subblock) coefficient values obeyed a Laplacian distribution [26], and designed a uniform scalar quantizer. The quantizer optimized the bit allocation among the different subbands by using an operational rate-distortion approach (minimizing the functional $D + \lambda R$) [33]. We then entropy-coded the resulting coefficient streams using a combination of zero-run-length coding and adaptive Huffman coding, as in the FBI's Wavelet Scalar Quantization standard [14].

We applied these different wavelet image coders to the Lena (NITF6) image, as well as a geometric test pattern, at a variety of compression ratios. The results are shown in Tables 4 and 5, and in Figures 13 and 14. On Lena, the Chui-Lian multiwavelet outperformed both the D_4 and (3,5) scalar wavelets, while the GHM multiwavelet was comparable with D_4 and outperformed (3,5) at compression ratios of 32:1 and 64:1. The images in Figure 13 show that both the approximation-based multiwavelet schemes produce fewer Cartesian artifacts than the scalar wavelet, and the Chui-Lian multiwavelet preserves more detail (e.g. the eyelashes). The adjacent-row method did not work well on *Lena*. However, the adjacent-row method did do well on the geometric test pattern image (Figure 14) with the constrained pair #1 "CP-1" outperforming D_4 (and GHM with approximation) at the 8:1 compression ratio. When using the repeated row algorithm, the constrained pairs significantly outperformed the GHM symmetric multiwavelet, demonstrating the importance of the eigenvector constraints (14) - (15). A close look at the details of the compressed/decompressed test patterns shows that the CP-1 compression "rang" over a shorter distance than the D_4 compression. While the (3,5)-tap scalar wavelet produced minimal ringing,

it significantly degraded the checkerboard pattern. The Chui-Lian multiwavelet did the best, yielding a lossless (!) compression at 8:1 and beating all contenders at all compression ratios.

These preliminary results suggest that multiwavelets are worthy of further investigation as a technique for image compression. Issues to address include the design of multiwavelets with symmetry and higher order of approximation than the GHM system, the role of eigenvector constraints, and also further exploration of regularity for multiwavelets [42]. One might also apply zerotree-coding methods [32] in a multiwavelet context. Other interesting results on implementation of multiwavelets for image compression can be found in [7].

Compression Ratio	8:1	16:1	32:1	64:1
	pSNR	pSNR	pSNR	pSNR
(3,5)-tap scalar QMF	37.6	33.1	30.2	27.1
Daubechies 4	38.0	34.6	31.3	28.41
GHM with appr./deappr.	37.5	34.0	31.1	28.5
Chui-Lian with appr./deappr.	38.3	34.7	31.5	28.4
constrained pair #1	35.3	31.1	27.9	25.5
constrained pair #2	34.4	30.4	27.3	24.9

Table 4: Peak SNRs for compression of *Lena*.

Compression Ratio	8:1	16:1	32:1	64:1
	pSNR	pSNR	pSNR	pSNR
(3,5)-tap scalar QMF	63.8	36.2	23.1	16.5
Daubechies 4	78.2	44.9	31.5	21.8
GHM with appr./deappr.	56.7	35.7	27.2	22.2
Chui-Lian with appr./deappr.	∞	57.3	37.0	27.3
constrained pair 1	91.2	41.6	29.2	21.8
constrained pair 2	53.6	34.6	24.8	21.1

Table 5: Peak SNRs for compression of geometric test pattern.

Original Lena image

(3,5)-tap scalar wavelet
32:1 compression, pSNR 30.2

Daubechies 4
32:1 compression, pSNR 31.3

Constrained Pair #1
32:1 compression, pSNR 27.9

GHM with approximation
32:1 compression, pSNR 31.1

Chui-Lian with approximation
32:1 compression, pSNR 31.5

Figure 13: Wavelet and multiwavelet compression of Lena image.

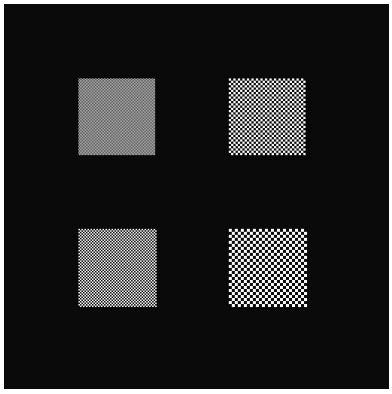

Original geometric pattern

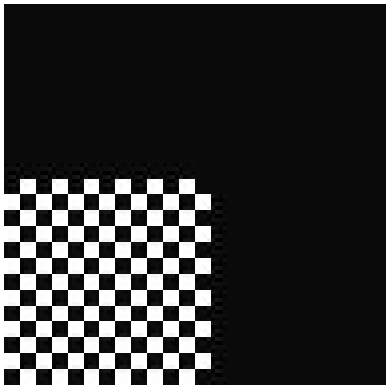

Detail of original pattern

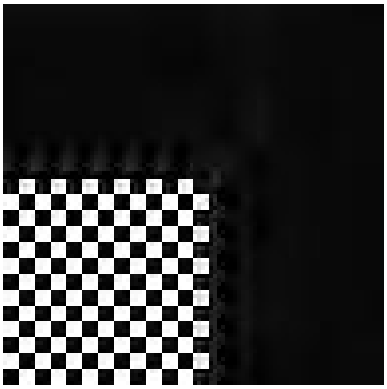

Daubechies 4 scalar wavelet compression (32:1, pSNR 31.52)

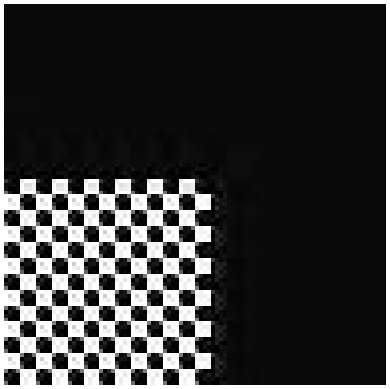

Biorthogonal 3-5 scalar compression (32:1, pSNR 23.05)

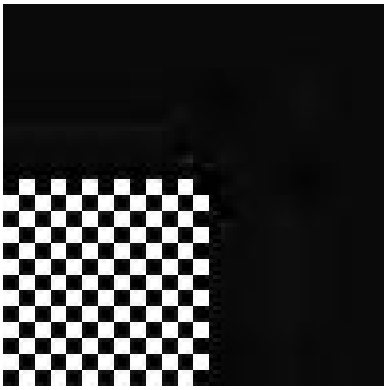

Chui-Lian with approximation multiwavelet compression (32:1, pSNR 37.04)

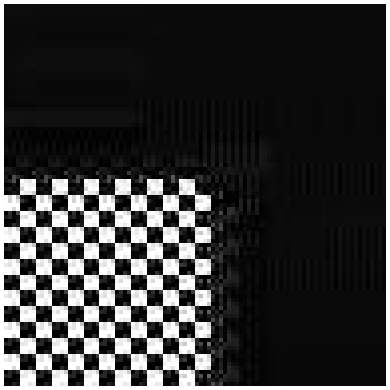

Constrained pair #1 adjacent row multiwavelet compression (32:1, pSNR 29.16)

Figure 14: Wavelet and multiwavelet compression of geometric pattern.

7 Conclusions

After reviewing the recent notion of multiwavelets (matrix-valued wavelet systems), we have examined the use of multiwavelets in a filter bank setting for discrete-time signal processing. Multiwavelets offer the advantages of combining symmetry, orthogonality, and short support, properties not mutually achievable with scalar 2-band wavelet systems. However, multiwavelets differ from scalar wavelet systems in requiring two or more input streams to the multiwavelet filter bank. We described two methods (repeated row and approximation/deapproximation) for obtaining such a vector input stream from a one-dimensional signal. We developed the theory of symmetric extension for multiwavelet filter banks, which matches nicely with approximation-based preprocessing. Moving on to two-dimensional signal processing, we described an additional algorithm for multiwavelet filtering (two rows at a time), and developed a new family of multiwavelets (the constrained pairs) that is well-suited to this two-row-at-a-time filtering.

We then applied this arsenal of techniques to two basic signal processing problems, denoising via thresholding (wavelet shrinkage), and data compression. After developing the approach via model problems in one dimension, we applied the various new multiwavelet approaches to the processing of images, frequently obtaining performance superior to the comparable scalar wavelet transform. These results suggest that further work in the design and application of multiwavelets to signal and image processing is well warranted.

Acknowledgments: We would like to thank Scott Hills for help programming the image compressions, and Stephane Mallat for useful discussions.

References

[1] B. Alpert, "A class of bases in L^2 for the sparse representation of integral operators," *SIAM J. Math. Analysis,* vol. 24, 1993.

[2] M. Antonini, M. Barlaud, P. Mathieu, and I. Daubechies, "Image coding using the wavelet transform," *IEEE Trans. on Image Processing,* vol. 1, pp. 205-220, 1992.

[3] R. H. Bamberger, S. L. Eddins, and V. Nuri, "Generalized symmetric extension for size-limited multirate filter banks," *IEEE Trans. on Image Proc.,* vol. 3, pp. 82-86, 1994.

[4] C. Brislawn, "Classification of symmetric wavelet transforms," Los Alamos Technical Report, 1993.

[5] B. V. Brower, "Low-bit-rate image compression evaluations," *Proc. SPIE*, Orlando, FL, April 4-9, 1994.

[6] C. K. Chui and J. A. Lian "A Study of Orthonormal Multiwavelets," *J. Appl. Numer. Math.*, vol. 20, pp. 272-298, 1996.

[7] M. Cotronei, L. B. Montefusco, and L. Puccio, "Multiwavelet analysis and signal processing," *IEEE Trans. on Circuits and Systems II*, to appear.

[8] T. Downie and B. Silverman, "The discrete multiple wavelet transform and thresholding methods," *IEEE Trans. on Signal Proc.*, to appear.

[9] W. Dahmen, B. Han, R.-Q. Jia, and A. Kunoth, "Biorthogonal multiwavelets on the interval: cubic Hermite splines," preprint, 1998.

[10] I. Daubechies, *Ten Lectures on Wavelets*, Philadelphia: SIAM, 1992.

[11] D. Donoho, "De-noising by soft-thresholding," *IEEE Trans. Inf. Theory,* vol. 41, pp. 613-627, 1995.

[12] D. L. Donoho and I. M. Johnstone, "Ideal spatial adaptation via wavelet shrinkage," *Biometrika,* vol. 81, pp. 425-455, 1994.

[13] G. Donovan, J. Geronimo, and D. Hardin, "Intertwining multiresolution analyses and the construction of piecewise polynomial wavelets," *SIAM J. Math. Anal.*, vol. 27, pp. 1791-1815, 1996.

[14] Fed. Bureau of Investig., *WSQ Gray-Scale Fingerprint Image Compression Specification,* drafted by T. Hopper, C. Brislawn, and J. Bradley, IAFIS-IC-0110-v2, Feb. 1993.

[15] V. M. Gadre and R. K. Patney, "Vector multirate filtering and matrix filter banks," *Proc. IEEE ISCAS*, San Diego, 1992.

[16] J. Geronimo, D. Hardin, and P. R. Massopust, "Fractal functions and wavelet expansions based on several functions," *J. Approx. Theory,* vol. 78, pp. 373-401, 1994.

[17] R. A. Gopinath, J. E. Odegard, and C. S. Burrus, "Optimal wavelet representation of signals and the wavelet sampling theorem," *IEEE Trans. on Circ. and Sys. II,* vol. 41, pp. 262-277, 1994.

[18] D. Hardin and J. Marasovich, "Biorthogonal multiwavelets on [-1,1]," preprint, 1997.

[19] D. Hardin and D. Roach, "Multiwavelet prefilters I: orthogonal prefilters preserving approximation order $p \leq 2$," preprint, 1997.

[20] C. Heil, G. Strang, and V. Strela, Approximation by translates of refinable functions," *Numerische Mathematik*, vol. 73, pp. 75-94, 1996.

[21] P. Heller, V. Strela, G. Strang, P. Topiwala, C. Heil, and L. Hills, "Multiwavelet filter banks for data compression," *Proc. IEEE ISCAS*, Seattle, WA, May 1995.

[22] Q. Jiang, "Parametrization of M-channel orthogonal multifilter banks," preprint, 1997.

[23] H. Kiya, K. Nishikawa, and M. Iwahashi, "A Development of symmetric extension method for subband image coding," *IEEE Trans. on Image Proc.,* vol. 3, pp. 78-81, 1994.

[24] W. Lawton, S. L. Lee, and Z. Shen, "An algorithm for matrix extension and wavelet construction," *Mathematics of Computation, Math. Comp.*, vol. 65, pp. 723-737, 1996.

[25] J. Lebrun and M. Vetterli, "Balanced multiwavelets: theory and design," *Proc. IEEE ICASSP,* Munich, 1997.

[26] S. Mallat, "A theory for multiresolution signal decomposition: the wavelet representation," *IEEE Trans. PAMI,* vol. 11, pp. 674-693, 1989.

[27] J. Miller and C. Li, "Adaptive miltiwavelet initialization," preprint 1997.

[28] J. Odegard, M. Lang, H. Guo, R. Gopinath, and C. Burrus, "Nonlinear wavelet processing for enhancement of images," submitted to *IEEE SP Letters,* 1994.

[29] G. Plonka, "Approximation order provided by refinable function vectors," *Const. Approx.*, vol 13, pp. 221-244, 1997.

[30] G. Plonka, "Generalized spline wavelets," *Constr. Approx.*, vol. 12, pp. 127-155, 1996.

[31] G. Plonka and V. Strela, "Construction of multi-scaling functions with approximation and symmetry," *SIAM J. Math. Anal.*, to appear.

[32] J. M. Shapiro, "Embedded image coding using zerotrees of wavelet coefficients," *IEEE Trans. on SP,* vol. 41, pp. 3445-3662, 1993.

[33] Y. Shoham and A. Gersho, "Efficient bit allocation for an arbitrary set of quantizers," *IEEE Trans. ASSP*, vol. 36, pp. 1445-1453, 1988.

[34] M. J. T. Smith and S. Eddins, "Analysis-synthesis techniques for subband image coding," *IEEE Trans. ASSP,* vol. 38, pp. 1446-1456, 1990.

[35] G. Strang and T. Nguyen, *Wavelets and Filter Banks*, Wellesley, MA: Wellesley-Cambridge Press, 1995.

[36] G. Strang and V. Strela, "Short wavelets and matrix dilation equations," *IEEE Trans. on SP,* vol. 43, pp. 108-115, 1995.

[37] G. Strang and V. Strela, "Orthogonal multiwavelets with vanishing moments," *J. Optical Eng.,* vol. 33 , pp. 2104-2107, 1994.

[38] V. Strela, "A Note on Construction of Biorthogonal Multi-scaling Functions," in *Contemporary Mathematics*, A. Aldoubi and E. B. Lin (eds.), AMS 1998.

[39] V. Strela and G. Strang, "Finite element multiwavelets," *Proc. NATO Conference, Maratea,* Boston, MA: Kluwer, 1995.

[40] V. Strela and A. T. Walden, "Signal and image denoising via wavelet thresholding: orthogonal and biorthogonal, scalar and multiple wavelet transforms," *Statistics Section Technical Report TR-98-01, Dep. of Math., Imperial College, London*, 1998.

[41] G. Uytterhoeven, *Multiwavelets for image compression*, Masters thesis, Katholieke Universiteit Leuven, May, 1994.

[42] M. Vetterli and G. Strang, "Time-varying filter banks and multiwavelets," Sixth IEEE DSP Workshop, Yosemite, 1994.

[43] M. Vrhel and A. Aldroubi, "Projection based pre-filtering for multiwavelet transforms," preprint, 1997.

[44] X.-G. Xia, " A new prefilter design for discrete multiwavelet transforms," preprint, 1996.

[45] X.-G. Xia, J. Geronimo, D. Hardin, and B. Suter, "Computations of multiwavelet transforms," *Proc. SPIE 2569,* San Diego, CA, July 1995.

[46] X.-G. Xia, J. Geronimo, D. Hardin, and B. Suter, "Design of prefilters for discrete multiwavelet transforms," *IEEE Trans. on Signal Proc.*, vol. 44, pp25-35, 1996.

[47] W. Zettler, J. Huffman, and D. Linden. "The application of compactly supported wavelets to image compression," *Proc. SPIE* **1244***,* pp. 150-160, 1990.